ADVANCED FUNCTIONAL MATERIALS
www.afm-journal.de

Grayscale to Multicolor Laser Writing Inside a Label-Free Metal-Organic Frameworks

*Nikolaj A. Zhestkij, Anastasiia S. Efimova, Yuliya Kenzhebayeva, Svyatoslav A. Povarov, Pavel V. Alekseevskiy, Sergey S. Rzhevskiy, Sergei A. Shipilovskikh, and Valentin A. Milichko**

Direct laser writing (DLW), being a universal tool for fast creating colorless/color images on different substrates, still suffers from simultaneous writing grayscale and color images inside the transparent media. Here, it is discovered that a unique set of porosity, coordination bonding between organic and inorganic building blocks, and the lack of inversion symmetry of the label-free metal-organic frameworks (MOFs), on the one hand, provides the possibility of laser writing the grayscale images through the amorphization/carbonization. On the other hand, the reduction of the laser writing power leads to controllable creation of color images via defect formation with sub-diffraction resolution inside the MOF crystals. The latter is due to the processes of self-absorption of generated optical harmonics by nonlinear MOFs within the visible spectral range. As a result, simultaneous grayscale and multicolor writing of QR codes and images are demonstrated with up to 400 nm resolution inside optically transparent MOF crystals, thereby discovering a new family of functional materials for DLW.

1. Introduction

Direct laser writing (DLW) is an industry-oriented method for creating the images both on the surface and in the volume of various media[1] for nanophotonic, medicine, bioengineering, and even IT applications.[2] Possessing a high energy efficiency and processing speed,[3] DLW allows one to remotely create grayscale or color images for informational purposes or encryption, as well as to guide optical signals via optical circuits and passive optical elements at macro and nano scales.[4] Next to the above advantages of DLW, the method is also unique in terms of non-destructive thermal effect, an ability to create grayscale or color images, demonstrating better color depth[5a] and high stability over time,[5b] compared to conventional chemical coloring. In the latter case, the color is coming from periodic structures and photonic crystals formed by DLW,[6a–d] plasmonic nanostructures,[6e,f] and photothermal oxidation of the material.[5a,6g] However, the challenges on the creation of color images with sub-diffraction resolution inside the media,[6h] as well as the impossibility of achieving black and grayscale shades simultaneously with full color palette significantly hinder the widespread use of DLW.

Staying in the laser writing paradigm, we have proposed a new concept for simultaneous multicolor and grayscale writing inside the media with sub-diffraction resolution through the use of a whole class of non-linear optical (NLO) metal-organic frameworks (MOFs).[7] Being a family of coordination polymers, MOFs are formed by strong and weak chemical interactions between the organic and inorganic building blocks, resulting in porous crystalline structure with a great chemical and structural diversity. The combination of these properties allows utilizing MOFs for gas sorption, catalysis, sensing, microelectronics, and photonics.[8] Intriguing is that a unique set of MOF properties such as organic-inorganic nature and coordination bonding underlies a new laser-assisted method for obtaining MOF functional derivatives[9] and even laser writing. Nevertheless, MOFs have been considered yet as a crystalline container for guests (dyes, metal ions) to obtain independently grayscale[10a] or color[10b–d] images.

In contrast, we discovered that the set of porosity, coordination bonding between organic and inorganic building blocks, and the lack of inversion symmetry of MOFs, on the one hand, provides the possibility of laser writing the grayscale images through the amorphization/carbonization (harsh laser writing mode); on the other hand, the reduction of the laser writing power (gentle laser writing mode) leads to controllable creation of color images via defect formation with sub-diffraction resolution inside the MOF crystals. The latter is due to the process of self-absorption of generated second optical harmonics by NLO MOFs within the visible spectral range. As a result, we have demonstrated the controllable process of simultaneous grayscale and multicolor writing of QR codes and images with 400 nm resolution inside optically transparent and label-free MOF crystals, thereby discovering a new family of functional materials for DLW.

N. A. Zhestkij, A. S. Efimova, Y. Kenzhebayeva, S. A. Povarov, P. V. Alekseevskiy, S. S. Rzhevskiy, S. A. Shipilovskikh, V. A. Milichko
School of Physics and Engineering
ITMO University
St. Petersburg 197101, Russia
E-mail: v.milichko@metalab.ifmo.ru

The ORCID identification number(s) for the author(s) of this article can be found under https://doi.org/10.1002/adfm.202311235

DOI: 10.1002/adfm.202311235

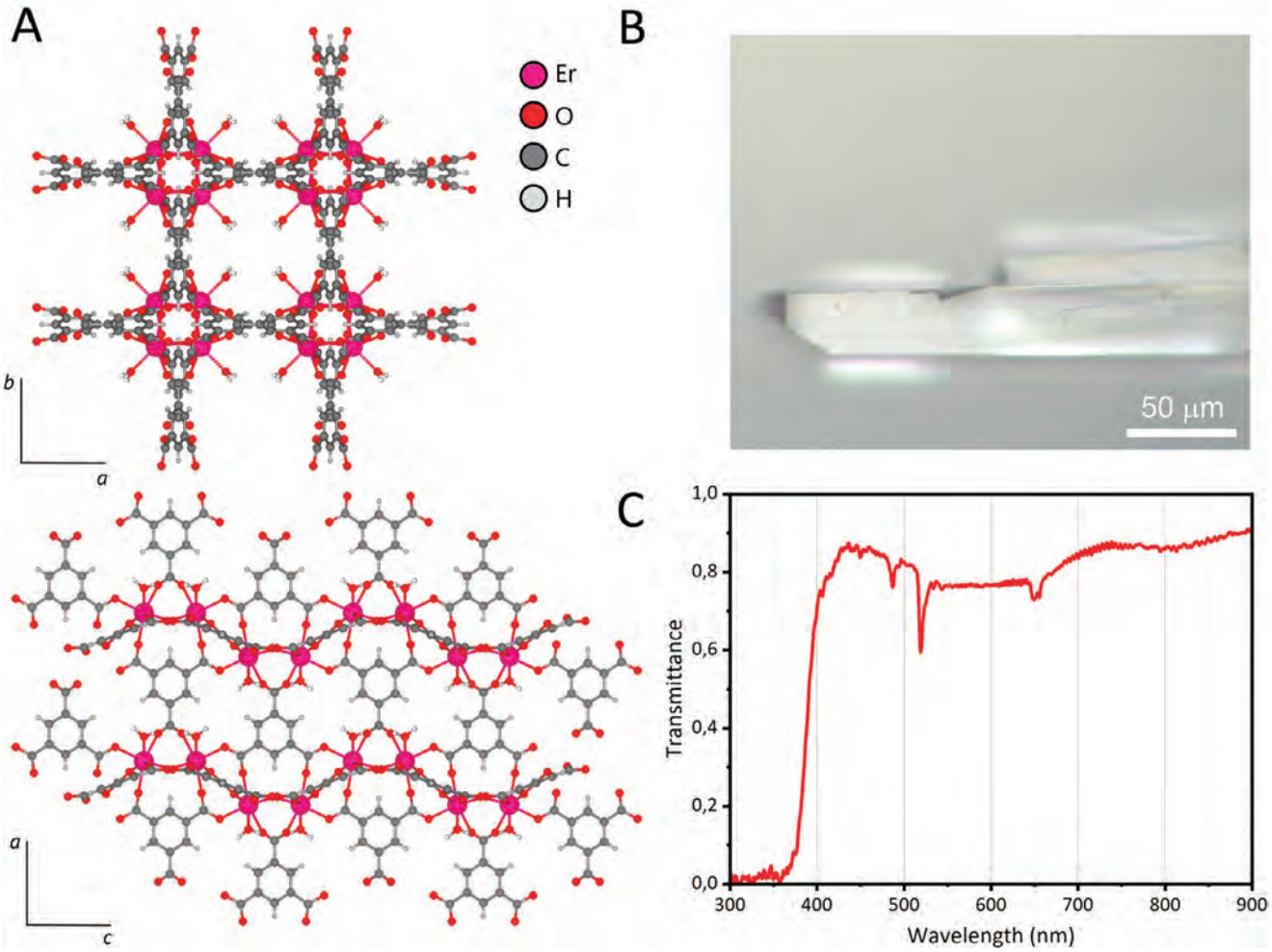

Figure 1. A) Er-BTC MOF structure[7m] with corresponding optical image B). C) Transmittance spectrum for Er-BTC single crystal of 100 μm thick.

2. Results and Discussion

Following the concept, according to which MOF (a hierarchical structure based on organic and inorganic blocks linked together via coordination bonding)[11a] should possess NLO properties (via lack of inversion symmetry), we have considered the recently reported model NLO MOF.[7m] Such Er-BTC crystals (BTC = 1,3,5-benzenetricarboxylic acid) demonstrate noncentrosymmetric structure ($P4_122$ space group, **Figure 1**A), providing high values of second-order nonlinear susceptibility $\chi^{(2)}$ (experimental analysis[7m] and calculation of static values of $\chi^{(2)}$ revealed that $\chi^{(2)}$ for Er-BTC is equal to $0.5*\chi^{(2)}$ for urea, see Table S2, Supporting Information), porosity (0.24 $cm^3\ g^{-1}$, calc. accessible void volume of 625 $Å^3$ which is 41.5% of the unit cell volume), thermal stability (up to 270 °C, see Figure S1, Supporting Information), as well as optical transparency window from 400 to 900 nm (Figure 1B,C).

To realize DLW, we have used optical parametric amplifier (OPA) laser system with tunable parameters occupied with Orpheus-F and Orpheus-HP light conversion systems (325 to 2500 nm and 315 to 2600 nm, 200 fs pulse duration) in order to obtain 2 laser writing modes: a harsh laser writing mode (**Figure 2**A) that can be realized with 0.05 to 1 μJ laser pulses with 0.1 Hz to 1 MHz repetition rates, and a gentle laser writing mode (**Figure 3**A) at app. 0.2 μJ laser pulses with kHz repetition rate.

As one can see in Figure 2C–E; Figure S6 (Supporting Information) the laser writing of the grayscale QR codes on the surface and inside the volume of the MOF crystal of 100 μm thick has been performed by 1030 nm laser pulses focused by an objective with a numerical aperture (NA) of 0.9. Such QR codes have been obtained by 0.2 μJ laser pulses with 0.1 Hz repetition rate. The confocal Raman spectroscopy (Figure 2B; Figures S3, and S4, Supporting Information) of the obtained QR codes revealed the spatial resolution of individual grayscale dot (app. 1 μm), as well as confirmed the amorphization and coordination bond breaking at 0.2 μJ laser pulses with 0.1 Hz repetition rate. Herein, the black dots appeared after the DLW at 0.05 μJ laser pulses with 1 MHz repetition rate can be attributed the carbonization. In addition, with this harsh laser writing mode (changing only the pulse energy at a fixed repetition rate, and regardless of the laser wavelength), the identical images with different contrast (Figure S5, Supporting Information) have been also obtained, confirming the possibility of the grayscale writing.

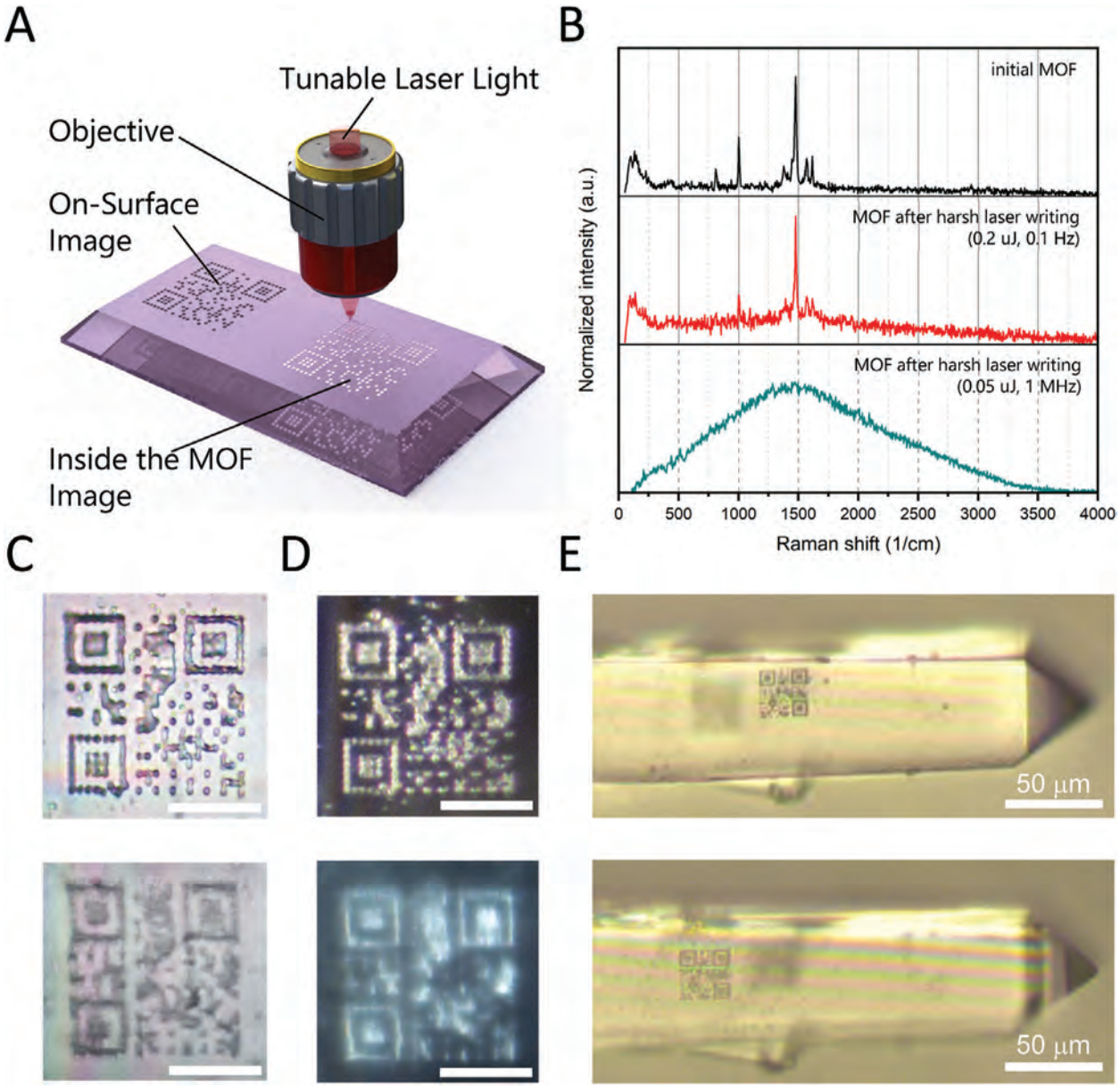

Figure 2. A) Scheme of harsh laser writing of grayscale images. B) Raman spectra from the initial MOF (Er-BTC) single crystal, as well the crystal after harsh laser writing at 0.2 μJ laser pulses with 0.1 Hz repetition rate and 0.05 μJ laser pulses with 1 MHz repetition rate. C) Bright field and D) dark field optical images of grayscale QR code on the MOF surface (upper) and the volume (down), obtained by 0.2 μJ laser pulses with 0.1 Hz repetition rate. Scale bar, 10 μm. E) Er-BTC single crystal with grayscale QR codes obtained by 0.2 μJ laser pulses with 0.1 Hz repetition rate on the surface and inside the MOF volume.

To switch to color regime, the gentle laser writing mode has been utilized. For this, 0.2 μJ laser pulses at kHz repetition rate and 850 to 1300 nm wavelengths (Figure S8, Supporting Information) passed through the NLO MOF single crystal of 100 μm thick. As a result, the generation of second optical harmonics (SHG, ranging from 425 to 650 nm, see Figure 3A) allowed us to precisely obtain different multicolor images (Figure 3B,D; Figure S7, Supporting Information) and dots (Figure S8, Supporting Information) with an extended color palette inside an optically transparent MOF.

In order to confirm the importance of non-centrosymmetric structure of MOFs for the controlled creation of dots with a given color at the desired location, we have also utilized two optically transparent and centrosymmetric MOFs based on Zr (UiO-66) and Tb ions.[13f] As shown in Figure S12 (Supporting Information) for Tb-based MOF, we were able to randomly and uncontrollably create some color shapeless dots. However, enumerating the laser writing modes for UiO-66 did not allow obtaining color dots at all (and when a certain threshold of the laser pulse energy has been reached, the MOFs carbonized and degraded).[9d] This allows us to speculate that the lack of inversion symmetry of MOFs supports nonlinear generation of optical harmonics, which can be then effectively absorbed through two-photon absorption by an optically transparent NLO MOF (Figure 1C).

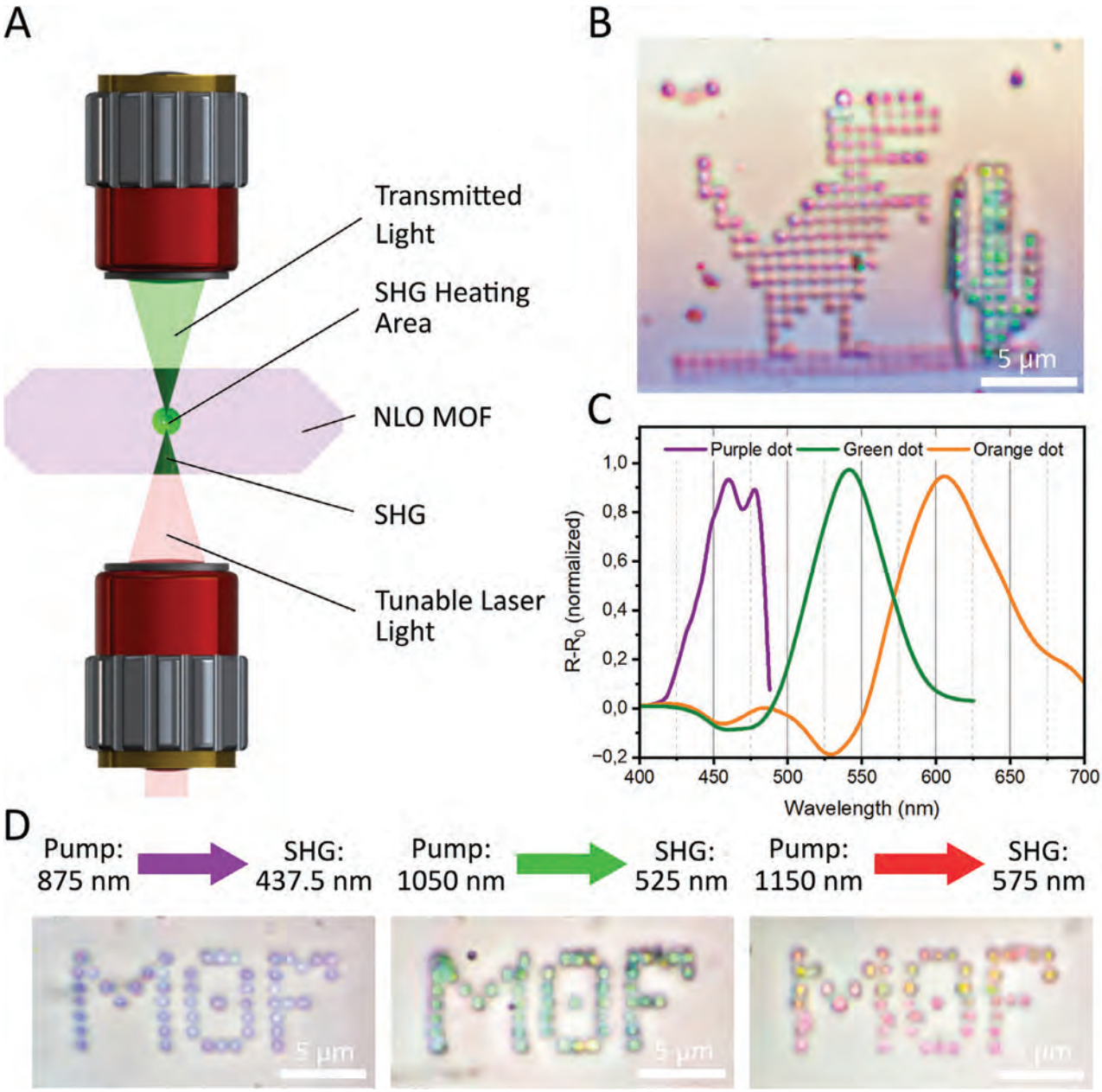

Figure 3. A) Scheme of gentle laser writing of multicolor images. B) Simultaneous multicolor image with corresponding spectra of a white light scattering C). D) The color dots (purple to orange) obtained with the corresponding SHG wavelengths (437.5 to 575 nm).

We considered that such nonlinear SHG process facilitated the absorption of photon (with the wavelengths of 425 to 650 nm, compared to 850 to 1300 nm of the incoming light) and converting their energy to heat in the local laser focus area. Herein, one cannot exclude another NLO process (generation of third optical harmonics, THG, which also occurs in centrosymmetric structures) for creating multicolor images (Figure S12, Supporting Information). However, an efficiency of THG process is usually less than that of SHG,[11f] and also requires deep infrared pumping to get the THG wavelengths into the transparency window of MOFs.

The obtained multicolor images have been studied then by confocal Raman spectroscopy (**Figure 4**), which revealed the following: The color images and dots, both in the image plane (Figure 4A) and in the depth (Figure 4B), are characterized by amorphization of the framework (disappearance of the ligand peaks and growth of an amorphous halo, Figure 4C,D). Herein, the Raman spectra are identical regardless of the color of the image. However, the size of the amorphized area inside the MOF is already depend on the SHG wavelength (Figure 4E,F) and the laser focusing parameters: For instance, the purple dot in Figures 3D, 4A possessed 0.8 μm in diameter (Figure S10, Supporting Information) and 2 μm of thick. This analysis allowed us also to speculate that the specific features of the thermal conductivity of MOFs (namely, low concentration of phonons and limited speed of their propagation, determined by weak chemical

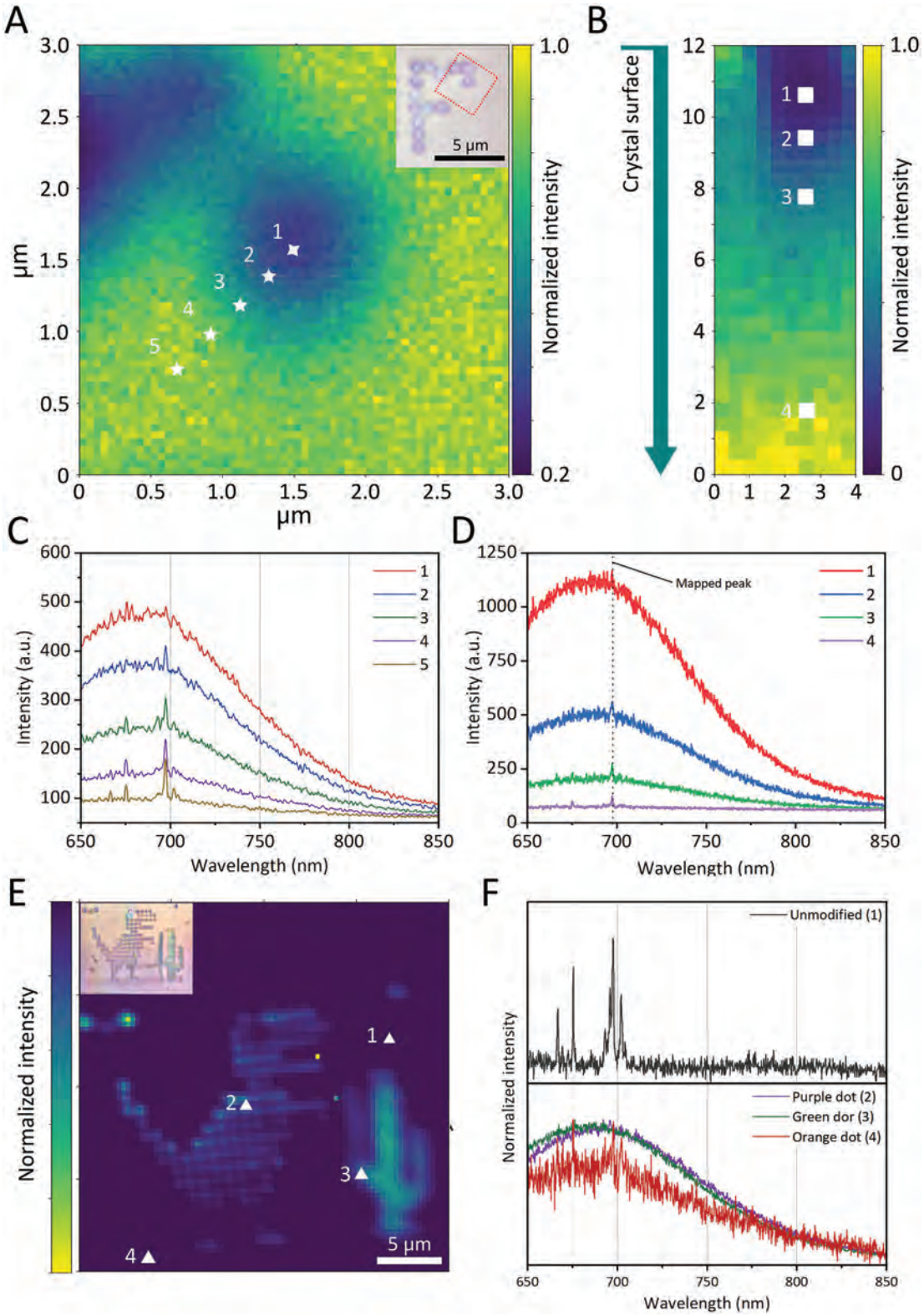

Figure 4. A) Confocal Raman mapping of purple dots from Figure 3D in the plane (optical image in inset) with corresponding Raman spectra C). B) Confocal Raman mapping of purple dot from Figure 3D in the depth with corresponding Raman spectra D). E,F) Confocal Raman mapping of the image in Figure 3B in the plane (optical image in inset) with corresponding Raman spectra of the selected points.

Table 1. MOFs for DLW of grayscale/color images.

Type	Mechanism of DLW	MOF	Laser source (wavelength, nm)	Resolution [μm]	Refs.
Grayscale	Two photon polymerization	Ag ions in MOF-5	780	0.7	[10a]
Color		DMOF ⊃ DETC-PEGDA	800	0.6	[10b]
		MOF-5 ⊃ DEPC-PEGDA, MOF-5 ⊃ Coumarin 6-PEGDA, MOF-5 ⊃ 4-Di-2-ASP-PEGDA	800	0.4	[10c]
		ZJU-56–0.20	365	2	[10d]
Grayscale and multicolor	MOF structural deformation	Er-BTC	850 – 1300	0.40 ± 0.02	This work

bonding between organic and inorganic building blocks)[11b–e] ensured the localization of heat inside the laser focusing area. The latter contributed to an effective amorphization and corresponding color changes on the scale of this area. Therefore, the diameter of these local areas could be commensurate with the diffraction limit ($1.22\lambda/n$NA) and equal 0.42 ± 0.04, 0.51 ± 0.05, and 0.56 ± 0.06 μm (for 437.5, 530, and 574 nm SHG wavelength, λ, respectively; NA equals 0.7), while the refractive index of amorphized MOF, n, can vary from 1.6 to 2.[12] As a result, one can obtain purple, green, and orange dots inside the MOF crystal corresponding to 437.5 nm, 530 nm, and 574 nm SHG wavelengths (Figure 3B,D), confirmed also by white light scattering spectroscopy (Figure 3C) revealing the efficient scattering of 460, 540, and 600 nm light.

In addition, a combination of confocal Raman mapping with a step of 50 nm (demonstrating an average 0.8 μm size of color dots, Figure 4; Figure S10, Supporting Information), diffraction approximation (reporting on 0.42 to 0.56 μm) and also profile intensity measurement (revealing 0.4 to 0.66 μm, Figure S9, Supporting Information) showed that the gentle laser writing mode allows achieving up to 400 nm size of color dots with app. 1.25 μm distance between them. Nevertheless, the thermal nature of the creation of color dots gives them a loose boundary (Figure 4A,B; Figure S10, Supporting Information), which blurs their physical size.

Next, we have checked the morphology of the MOF surface after DLW: the laser writing of the color dots (in Figure 3B), located at the distance of app. 1 μm from each other, caused no morphological changes on the MOF surface (as confirmed by atomic force microscopy, Figure S11, Supporting Information). Moreover, an analysis of the stability of QR codes and such multicolor images revealed 100% safety of the images and color rendition after 6 months storage under ambient conditions.

To discuss the results obtained, we refer to previous works on MOFs where they have been considered as a media for DLW (**Table 1**).[10] In that cases, the frameworks have been filled or incorporated with the light sensitive polymers or reagents followed by polymerization via two-photon absorption process. The formation of 2- to 3D grayscale or color images with 400 to 700 nm resolution has been achieved then by removing unreacted polymer with a solvent. Herein, in our case, no any specific modification of MOFs is required (i.e., label-free frameworks), and simultaneous writing of grayscale and multicolor images with 400 nm resolution (**Figure 5**) has been achieved through nonlinear optical processes of light conversion (light absorption in order to achieve carbonization, and SHG heating to induce the local amorphization). Moreover, the writing of grayscale and black dots (Figure 5D) is wavelength independent and regulated only by the ratio of laser pulse energy and repetition rate (Figure 5C), while the writing of a specific color (Figure 5E) depends directly on the wavelength at a fixed repetition rate (Figure 5C). It should be noted that the spatial resolution can be also downscaled up to 300 nm by utilizing an objective with a higher NA (i.e., 0.9 instead of 0.7). Finally, we proposed that the concept can be relevant for another NLO MOFs with an optical transparency, the list of which is currently wide (**Table 2**).[7a–c]

Looking beyond, the recent research in the field of materials for information encryption has shown that luminescent and NLO MOFs represent a new class of functional materials for storing and transmitting the information (in the form of QR codes, labels, or dynamic images) encrypted in the color that specific MOF generates.[13a–g] Therefore, our results extend these capabilities by increasing the number of colors that can be created simultaneously by DLW on MOF with sub-diffraction resolution, thereby resulting in an increased data packing via color QR codes and enabling the creation of unclonable multicolor labels for goods protection,[13h,i] which are robust at ambient conditions. To prove this, we used slight differences in the color of the obtained orange dots ("dinosaur" from Figure 3B). Indeed, as it was demonstrated in the experiment (Figure 3C; Figure S13, Supporting Information), the peak positions of scattering light for dots obtained with the same writing parameters can experience a random spectral shift up to 20 nm. Such shift can be explained by fluctuations in the laser writing conditions (e.g., inhomogeneity of the laser illumination, irregularities in the MOF crystal, etc.) and can be distinguished using a spectrometer, even if the color of dots is visually the same. Thus, each uni- and multi-color image, in fact, is unique, as consists of pixels (dots) with randomized positions of the scattering spectra peaks. Such features can be used for creation of physically unclonable security labels, whichattracts a special attention in anti-counterfeiting applications.[14] In our case, the studies of scattering spectra showed that for each dot of similar color, there are at least 10 peak positions which can be recognized (Figure S13, Supporting Information). Moreover, preliminary estimation demonstrated that, to ensure sufficient encoding capacity of the MOF-based unclonable security label, it is enough to create the image consisting of 300 color dots[14a] (for more information, see Supporting Information).

3. Conclusion

We discovered that a unique set of porosity, coordination bonding between organic and inorganic building blocks, and the lack of

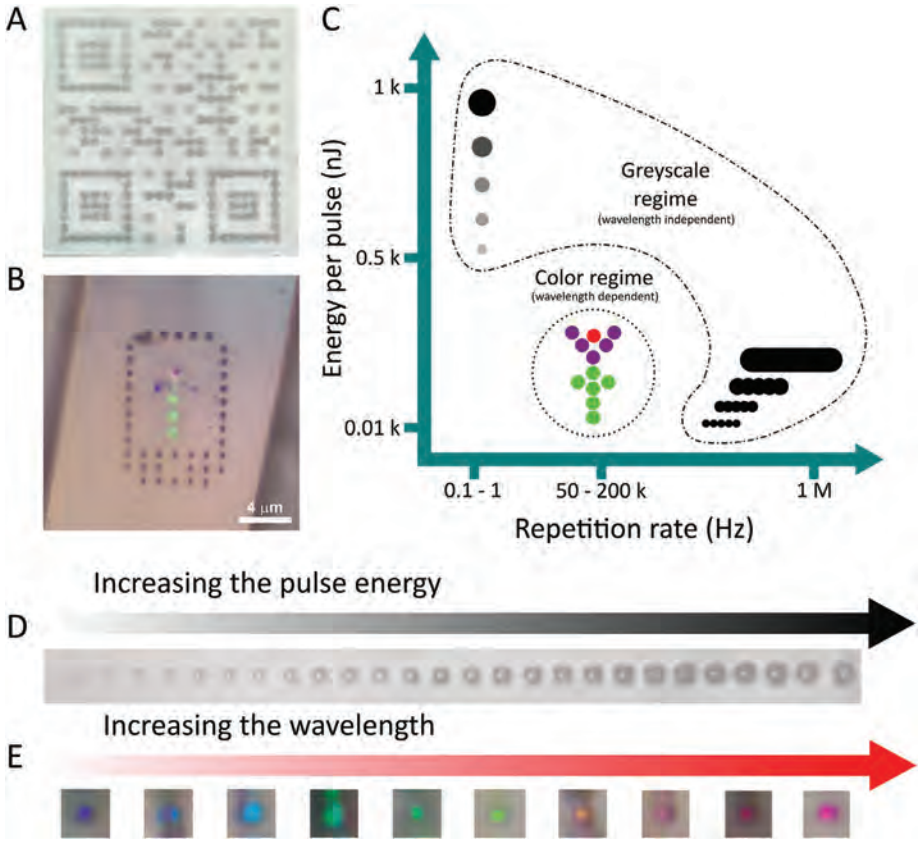

Figure 5. A) Grayscale QR code on the MOF surface encoding the term "MOF" (see also Figure S6, Supporting Information). B) Simultaneous DLW of color and black dots inside MOF. C) Scheme for selecting the laser writing mode (energy of the laser pulse versus the pulse repetition rate) for making color and grayscale images with corresponding evolution of the grayscale D), depending on the laser pulse energy (from 0.4 μJ to 1.8 μJ with 0.067 μJ step), and color E), depending on the laser wavelength (from 850 to 1300 nm with 50 nm step).

inversion symmetry of label-free MOFs, on the one hand, provides the possibility of laser writing the grayscale images through the amorphization/carbonization; on the other hand, the reduction of the laser writing power leads to controllable creation of multicolor images via amorphization with sub-diffraction resolution inside an optically transparent MOF crystals. The latter has been achieved due to the processes of self-absorption of generated optical harmonics by NLO MOFs within the visible spectral range. As a result, we have demonstrated the controllable process of simultaneous grayscale and multicolor writing of QR codes and images with 400 nm resolution inside the MOF crystals, thereby discovering a new family of functional materials for DLW.

Table 2. List of non-centrosymmetric MOFs with an optical transparency for potential grayscale/multicolor DLW.

MOF	Refs.
ZIF-8	[7d]
ZJU-28	[7e]
$[CH_3CH_2NH_3]Yb_{0.79}Er_{0.21}(HCOO)_4$	[7f]
$[Zn(pvb)_2]$ (pvb = *trans*-2-(4-pyridyl)−4-vinylbenzoate) $ZnC_{28}H_{20}N_2O_4$	[7g]
La-Tb-MOF	[7h]
[Zn(BPHY)(SA)]n (BPHY = 1,2-bis(4-pyridyl)hydrazine, H2SA = succinic acid)	[7i]
IAM	[7j]
ZnFDCA	[7k]
$[Eu_2L_2(DMF)(H_2O)_2]\cdot 2DMF\cdot H_2O$	[7l]

4. Experimental Section

Synthesis of MOF Single Crystals: MOFs have been obtained by a previously published method.[7m] For this, $Er(ClO_4)*6H_2O$ (0.084 mmol) has been dissolved in 1 mL of ethanol and 1 mL of distilled water, and 1,3,5-benzenetricarboxylic acid (0.084 mmol) has been dissolved in 1 mL of dimethylformamide (DMF) under ultrasound. Then, the solution mixture has been placed into 4 mL vial and hermetically sealed with a lid with a rubber septum to exclude the interaction with the external environment and create excess pressure in the vessel. The solution mixture has been heated to 90 °C and kept for 48 h. Then, the reaction mixture has been cooled down to room temperature. The resulting single crystals has been separated from the mother liquid by filtration, and repeatedly washed 5 times with mixture of $DMF/H_2O/EtOH$ (1/1/1). The washed single crystals have been dried in the air (CCDC 2 247 587).

Laser Writing: For all the laser writing modes the self-made confocal optical setup was utilized, based on OPA femtosecond tunable laser system. As the laser, two channel PHAROS femtosecond laser (Light-conversion, 1030 nm central wavelength, 200 fs pulse duration, 10 uJ energy per pulse, 10 W integral power at 1 MHz repetition rate) occupied with Orpheus-F (Light-conversion, 325 – 2500 nm) and Orpheus-HP

(Light-Conversion, 315 – 2600 nm)) has been utilized. The configuration of the scheme allows one to extract the main harmonic of PHAROS into free space or select the operating wavelength from the OPAs' spectral range. The pulse repetition rate has been regulated with PHAROS internal pulse picker, providing the repetition frequency reduction from 1 MHz (for harsh laser writing mode) down to 0.1 Hz and a single-pulse mode. The energy per pulse has been adjusted with a polarization attenuator, consisting of a half-wave plate and Glan-Taylor prism (Thorlabs), both with anti-reflection coatings for B-range (700–1100 nm). For the OPA path, the combination of short- and long-pass optical filters were used (Thorlabs FESH and FELH premium filters) to prevent the release of unconverted PHAROS main harmonic. Greyscale images have been created in the reflection geometry (Figure 2A) with the laser pulses from PHAROS (main harmonic) focused on the MOF crystal via the high-aperture objective (Mitutoyo Plan APO, 100x VIS HR, NA = 0.9). The laser pulse repetition rate has been set at 0.1 Hz and pulse energy has been reduced to 1 µJ and lower (Figure 5C). In contrast, the color laser writing has been realized via transmission geometry (Figure 3A), where the initial laser beam has been focused from the lower objective (Mitutoyo Plan APO, 100x NIR HR, NA = 0.7), while the image has been collected from the upper one (Mitutoyo Plan APO, 100x VIS HR, NA = 0.9). To achieve the maximum efficiency in second harmonic generation, the polarization of the initial beam has been adjusted with the half-wave plate. The OPA's wavelengths utilized for the color laser writing (875 nm, 1060 nm, and 1150 nm) possess the pulse energy less than 0.2 µJ per pulse. Both greyscale and color laser writing modes required the precise positioning of the MOF crystal, while the position of the objective focal spot remained fixed. To do this, a 3-axis Piezo stage with up to 1 nm accuracy was used(Piezo systems Jena, TRITOR 101). The Piezo stage has been used in remote control mode with a self-coded C# script for each pattern. The integral laser power has been controlled with Ophir photonics power meters, occupied with heat or semiconductor sensors (in terms of power range).

Microscopic Imaging: Microscopic images of MOF single crystals have been obtained using Karl Zeiss AxioImager A2m in bright- and dark-field regimes via the 100x objective.

Atomic Force Microscopy: The AFM scans have been performed by SmartSPM 1000 (AIST-NT) microscope in semi-contact mode at ambient conditions. As working cantilevers, PPP-NCSTAuD-10 (Nanosensors) with highly doped silicon and Au coating on the detector side, 140 kHz resonant frequency and 14 N m^{-1} force constant with 7 nm tip radius have been utilized.

Optical Spectroscopy: The Raman and Reflection spectroscopic measurements have been performed in reflection mode via an objective (Mitutoyo Plan APO, 100x VIS HR, NA = 0.9). Raman measurements have been implemented under excitation by a 632.8 nm He-Ne continuous laser radiation, while for the reflection measurements the white halogen lamp (Avantes Hal-s mini) has been used. The collecting signal has been transferred to Horiba Labram Spectrometer with 150 g mm^{-1} (and 600 g mm^{-1} for Raman) diffraction gratings and a water-cooling CCD camera (ANDOR instruments, iDus). In both cases, the MOF single crystals have been precisely positioned with AIST PI piezo-stage. For the Raman mapping procedure (with 50 nm step, Figure 4; Figures S3,S4, Supporting Information), the stage moved the MOF under the stationary laser beam position, allowing us to reach the map space resolution up to 0.01 µm.

Supporting Information

Supporting Information is available from the Wiley Online Library or from the author.

Acknowledgements

N.A.Z., A.S.E. contributed equally to this work. V.A.M. acknowledges the financial support from the Russian Science foundation (grant number 22-72-10027 "Flexible hybrid materials as active layer in memory devices") and Priority 2030 federal Academic Leadership Program. S.A.S. acknowledges the financial support by the Government of the Russian Federation through the ITMO Fellowship and Professorship Program. The Authors thank Prof. Andrey S. Potapov and Xiaolin Yu (Nikolaev Institute of Inorganic Chemistry) for providing Tb-based MOF (ref. [13f]), as well as Dr. Dmitry Zuev, Martin Sandomirskii and Elena Popova (ITMO University) for support in analysis of the information encryption.

Conflict of Interest

The authors declare no conflict of interest.

Data Availability Statement

The data that support the findings of this study are available from the corresponding author upon reasonable request.

Keywords

direct laser writing, grayscale, metal-organic frameworks, multicolor, sub-diffraction

Received: September 16, 2023
Revised: January 5, 2024
Published online:

[1] a) A. Selimis, V. Mironov, M. Farsari, *Microelectron. Eng.* **2015**, *132*, 83; b) J. Fischer, M. Wegener, *Laser Photon. Rev.* **2013**, *7*, 22; c) I. Bernardeschi, M. Ilyas, L. Beccai, *Adv. Intell. Syst.* **2021**, *3*, 2100051.

[2] a) C. B. Arnold, P. Serra, A. Piqué, *MRS Bull.* **2007**, *32*, 23; b) N. R. Schiele, D. T. Corr, Y. Huang, N. A. Raof, Y. Xie, D. B. Chrisey, *Biofabrication* **2010**, *2*, 032001; c) A. Awad, F. Fina, A. Goyanes, S. Gaisford, A. W. Basit, *Int. J. Pharm.* **2020**, *586*, 119594; d) J. Fischer, M. Wegener, *Opt. Mater. Exp.* **2011**, *1*, 614.

[3] a) Y. Li, M. Hong, *Laser Photon. Rev.* **2020**, *14*, 1900062; b) J. Geng, L. Xu, W. Yan, L. Shi, M. Qiu, *Nat. Commun.* **2023**, *14*, 565.

[4] a) S. Coelho, J. Baek, J. Walsh, J. J. Gooding, K. Gaus, *Nat. Commun.* **2022**, *13*, 647,. b) C. Wei, Z. Zhang, D. Cheng, Z. Sun, M. Zhu, L. Li, *Int. J. Extreme Manuf.* **2021**, *3*, 012003.

[5] a) J. Geng, L. Xu, W. Yan, L. Shi, M. Qiu, *Nat. Commun.* **2023**, *14*, 565; b) E. Sedghamiz, M. Liu, W. Wenzel, *Nat. Commun.* **2022**, *13*, 2115.

[6] a) S. Kinoshita, S. Yoshioka, J. Miyazaki, *Rep. Prog. Phys.* **2008**, *71*, 076401,. b) M. Deubel, G. Von Freymann, M. Wegener, S. Pereira, K. Busch, C. M. Soukoulis, *Nat. Mater.* **2004**, *3*, 444; c) K. K. Seet, V. Mizeikis, S. Matsuo, S. Juodkazis, H. Misawa, *Adv. Mater.* **2005**, *17*, 541; d) S. Wong, M. Deubel, F. Pérez-Willard, S. John, G. A. Ozin, M. Wegener, G. Von Freymann, *Adv. Mater.* **2006**, *18*, 541; e) A. Kristensen, J. K. W. Yang, S. I. Bozhevolnyi, S. Link, P. Nordlander, N. J. Halas, N. A. Mortensen, *Nat. Rev. Mater.* **2016**, *2*, 16088; f) X. Zhu, C. Vannahme, E. Højlund-Nielsen, N. A. Mortensen, A. Kristensen, *Nat. Nanotechnol.* **2016**, *11*, 325; g) H. Liu, W. Lin, M. Hong, *APL Photon.* **2019**, *4*, 051101; h) H. Wang, Y. Lei, L. Wang, M. Sakakura, Y. Yu, G. Shayeganrad, P. G. Kazansky, *Laser. Photon. Rev.* **2022**, *16*, 2100563.

[7] a) L. R. Mingabudinova, V. V. Vinogradov, V. A. Milichko, E. Hey-Hawkins, A. V. Vinogradov, *Chem. Soc. Rev.* **2016**, *45*, 5408; b) R. Medishetty, J. K. Zaręba, D. Mayer, M. Samoć, R. A. Fischer, *Chem. Soc. Rev.* **2017**, *46*, 4976; c) C. Wang, T. Zhang, W. Lin, *Chem. Rev.* **2012**, *112*, 1084; d) S. Van Cleuvenbergen, I. Stassen, E. Gobechiya, Y. Zhang, K. Markey, D. E. De Vos, C. Kirschhock, B. Champagne, T. Verbiest, M. A. Van Der Veen, *Chem. Mater.* **2016**, *28*, 3203; e) J. Yu, Y. Cui, C. Wu, Y. Yang, Z. Wang, M. O'Keeffe, B. Chen, G. Qian, *Angew.*

Chem., Int. Ed. **2012**, *51*, 10542; f) M. Runowski, D. Marcinkowski, K. Soler-Carracedo, A. Gorczyński, E. Ewert, P. Woźny, I. R. Martín, *ACS Appl. Mater. Interfaces* **2023**, *15*, 3244; g) Z. Chen, G. Gallo, V. A. Sawant, T. Zhang, M. Zhu, L. Liang, A. Chanthapally, G. Bolla, H. S. Quah, X. Liu, K. P. Loh, R. E. Dinnebier, Q. H. Xu, J. J. Vittal, *Angew. Chemie Int. Ed.* **2020**, *59*, 833; h) Y. Wan, J. Wang, H. Shu, B. Cheng, Z. He, P. Wang, T. Xia, *Inorg. Chem.* **2021**, *60*, 7345; i) J. S. Guo, G. Xu, X. M. Jiang, M. J. Zhang, B. W. Liu, G. C. Guo, *Inorg. Chem.* **2014**, *53*, 4278; j) X. Huang, Q. Li, X. Xiao, S. Jia, Y. Li, Z. Duan, L. Bai, Z. Yuan, L. Li, Z. Lin, Y. Zhao, *Inorg. Chem.* **2018**, *57*, 6210; k) L. L. Xu, H. F. Zhang, M. Li, S. W. Ng, J. H. Feng, J. G. Mao, D. Li, *J. Am. Chem. Soc.* **2018**, *140*, 11569; l) S. Sun, F. Wang, Y. Sun, X. Guo, R. Ma, M. Zhang, H. Guo, Y. Xie, T. Hu, *Ind. Eng. Chem. Res.* **2019**, *58*, 17784; m) Zhestkij, N. A., Efimova, A. S., Kenzhebayeva, Y., Dmitriev, M. V., Novikov, A. S., Yushina, I. D., Krylov, A., Timofeeva, M. V., Kulakova, A. N., Glebova, N. V., Krasilin, A. A., Shipilovskih, S. A., Milichko, V. A., *Adv. Opt. Mater.* **2023**, *11*, 2300881.

[8] a) J. Li, P. M. Bhatt, J. Li, M. Eddaoudi, Y. Liu, *Adv. Mater.* **2020**, *32*, 2002563; b) D. Yang, B. C. Gates, *ACS Catal.* **2019**, *9*, 1779; c) P. Kumar, A. Deep, K. H. Kim, *Trends Analyt. Chem.* **2015**, *73*, 39; d) I. Stassen, N. Burtch, A. Talin, P. Falcaro, M. Allendorf, R. Ameloot, *Chem. Soc. Rev.* **2017**, *46*, 3185; e) X. Yang, X. Lin, Y. S. Zhao, D. Yan, *Chem. A Europ. J.* **2018**, *24*, 6484; f) Y. Lv, Z. Xiong, H. Dong, C. Wei, Y. Yang, A. Ren, Z. Yao, Y. Li, S. Xiang, Z. Zhang, Y. S. Zhao, *Nano Lett.* **2020**, *20*, 2020; g) D. Kottilil, M. Gupta, S. Lu, A. Babusenan, W. Ji, *Adv. Mater.* **2023**, *35*, 2209094; h) J. Yu, Y. Han, L. Wang, Y. Liu, H. Zhang, X. Chen, X. Liu, Z. Wang, J. Hu, *Ultrafast Sci.* **2023**, *3*, 0030; i) N. K. Kulachenkov, M. O. Barsukova, P. V. Alekseevskiy, A. A. Sapianik, M. Sergeev, A. N. Yankin, A. A. Krasilin, S. V. Bachinin, S. A. Shipilovskikh, P. S. Poturaev, N. A. Medvedeva, E. S. Denislamova, P. S. Zelenovskiy, V. V. Shilovskikh, Y. A. Kenzhebayeva, A. Efimova, A. S. Novikov, A. Lunev, V. P. Fedin, V. A. Milichko, *Nano Lett.* **2023**, *22*, 6972; j) N. K. Kulachenkov, D. Sun, Y. A. Mezenov, A. N. Yankin, S. Rzhevskiy, V. Dyachuk, A. Nominé, G. Medjahdi, E. A. Pidko, V. A. Milichko, *Angew. Chem., Int. Ed.* **2020**, *59*, 15522; k) V. A. Milichko, S. V. Makarov, A. V. Yulin, A. V. Vinogradov, A. A. Krasilin, E. Ushakova, V. P. Dzyuba, E. Hey-Hawkins, E. A. Pidko, P. A. Belov, *Adv. Mater.* **2017**, *29*, 1606034; l) N. Kulachenkov, Q. Haar, S. Shipilovskikh, A. Yankin, J.-F. Pierson, A. Nominé, V. A. Milichko, *Adv. Funct. Mater.* **2022**, *32*, 2107949; m) D. J. Li, Q.-h. Li, Z.-R. Wang, Z.-Z. Ma, Z.-G. Gu, J. Zhang, *J. Am. Chem. Soc.* **2021**, *143*, 17162.

[9] a) S. Guo, M. Gao, W. Zhang, F. Liu, X. Guo, K. Zhou, *Adv. Mater.* **2023**, *35*, 2303065; b) N. K. Kulachenkov, S. Bruyere, S. A. Sapchenko, Y. A. Mezenov, D. Sun, A. A. Krasilin, A. Nominé, J. Ghanbaja, T. Belmonte, V. P. Fedin, E. A. Pidko, V. A. Milichko, *Adv. Funct. Mater.* **2020**, *30*, 1908292; c) L. R. Mingabudinova, A. S. Zalogina, A. A. Krasilin, M. I. Petrova, P. Trofimov, Y. A. Mezenov, E. V. Ubyivovk, P. Lönnecke, A. Nominé, J. Ghanbaja, T. Belmonte, V. A. Milichko, *Nanoscale* **2019**, *11*, 10155; d) E. V. Gunina, N. A. Zhestkij, M. Sergeev, S. V. Bachinin, Y. A. Mezenov, N. K. Kulachenkov, M. Timofeeva, V. Ivashchenko, A. S. Timin, S. A. Shipilovskikh, A. A. Yakubova, D. I. Pavlov, A. S. Potapov, J. Gong, L. Khamkhash, T. Sh. Atabaev, S. Bruyere, V. A. Milichko, *ACS Appl. Mater. Interfaces* **2023**, *15*, 47541.

[10] a) R. Ameloot, M. B. J. Roeffaers, G. De Cremer, F. Vermoortele, J. Hofkens, B. F. Sels, D. E. De Vos, *Adv. Mater.* **2011**, *23*, 1788; b) Y. Zhang, Y. Su, Y. Zhao, Z. Wang, C. Wang, *Small* **2022**, *18*, 2200514; c) Y. Zhang, Y. Su, X. Fan, B. Zhao, X. Hua, B. Dai, C. Wang, *Adv. Opt. Mater.* **2023**, *11*, 2300364; d) J. Yu, Y. Cui, C.-D. Wu, Y. Yang, B. Chen, G. Qian, *J. Am. Chem. Soc.* **2015**, *137*, 4026.

[11] a) T. D. Bennett, F.-X. Coudert, S. L. James, A. I. Cooper, *Nat. Mater.* **2021**, *20*, 1179; b) X. Qian, J. Zhou, G. Chen, *Nat. Mater.* **2021**, *20*, 1188; c) H. Babaei, M. E. DeCoster, M. Jeong, Z. M. Hassan, T. Islamoglu, H. Baumgart, A. J. H. McGaughey, E. Redel, O. K. Farha, P. E. Hopkins, J. A. Malen, C. E. Wilmer, *Nat. Commun.* **2020**, *11*, 4010; d) A. M. Evans, A. Giri, V. K. Sangwan, S. Xun, M. Bartnof, C. G. Torres-Castanedo, H. B. Balch, M. S. Rahn, N. P. Bradshaw, E. Vitaku, D. W. Burke, H. Li, M. J. Bedzyk, F. Wang, J.-L. Brédas, J. A. Malen, A. J. H. McGaughey, M. C. Hersam, W. R. Dichtel, P. E. Hopkins, *Nat. Mater.* **2021**, *20*, 1142; e) S. S. Sørensen, M. B. Østergaard, M. Stepniewska, H. Johra, Y. Yue, M. M. Smedskjaer, *ACS Appl. Mater. Interfaces* **2020**, *12*, 18893; f) R. W. Boyd, in *Nonlinear Optics*, Elsevier, Amsterdam, The Netherlands **2008**.

[12] a) M. Treger, A. Hannebauer, A. Schaate, J. L. Budde, P. Behrens, A. M. Schneider, *Phys. Chem. Chem. Phys.* **2023**, *25*, 6333; b) X. Chong, K.-J. Kim, P. R. Ohodnicki, E. Li, C.-H. Chang, A. X. Wang, *IEEE Sens. J.* **2015**, *15*, 5327; c) N. C. Keppler, K. D. J. Hindricks, P. Behrens, *RSC Adv.* **2022**, *12*, 5807; d) C. Li, Z. Li, J.-g. Liu, X.-j. Zhao, H.-x. Yang, S.-y. Yang, *Polymer* **2010**, *51*, 3851; e) N. Huo, W. E. Tenhaeff, *Macromol* **2023**, *56*, 2113; f) T. Han, Z. Yao, Z. Qiu, Z. Zhao, K. Wu, J. Wang, A. W. Poon, J. W. Y. Lam, B. Z. Tang, *Nat. Commun.* **2019**, *10*, 5483; g) S. Watanabe, K. Oyaizu, *Macromolecules* **2022**, *55*, 2252.

[13] a) H.-Q. Zheng, Y. Yang, Z. Wang, D. Yang, G. Qian, Y. Cui, *Adv. Mater.* **2023**, *35*, 2300177; b) J. W. Oh, S. Lee, H. Han, O. Allam, J. I. Choi, H. Lee, W. Jiang, J. Jang, G. Kim, S. Mun, K. Lee, Y. Kim, J. W. Park, S. Lee, S. S. Jang, C. Park, *Light Sci. App.* **2023**, *12*, 226; c) C. Zhang, B. Wang, W. Li, S. Huang, L. Kong, Z. Li, L. Li, *Nat. Commun.* **2017**, *8*, 1138; d) J. Wang, B. Song, J. Tang, G. Hu, J. Wang, M. Cui, Y. He, *Nano Res.* **2020**, *13*, 1614; e) J. Yu, Y. Han, L. Wang, Y. Liu, H. Zhang, X. Chen, X. Liu, Z. Wang, J. Hu, *Ultrafast Sci.* **2023**, *3*, 0030; f) X. Yu, A. A. Ryadun, D. I. Pavlov, T. Y. Guselnikova, A. S. Potapov, V. P. Fedin, *Angew. Chem., Int. Ed.* **2023**, *62*, 202306680; g) J.-X. Wang, Y. Wang, M. Almalki, J. Yin, O. Shekhah, J. Jia, L. Gutiérrez-Arzaluz, Y. Cheng, O. Alkhazragi, V. K. Maka, T. K. Ng, O. M. Bakr, B. S. Ooi, M. Eddaoudi, O. F. Mohammed, *J. Am. Chem. Soc.* **2023**, *145*, 15435; h) J. H. Kim, S. Jeon, J. H. In, S. Nam, H. M. Jin, K. H. Han, G. G. Yang, H. J. Choi, K. M. Kim, J. Shin, S.-W. Son, S. J. Kwon, B. H. Kim, S. O. Kim, *Nat. Electron* **2022**, *5*, 433; i) T. Zhang, L. Wang, J. Wang, Z. Wang, M. Gupta, X. Guo, Y. Zhu, Y. C. Yiu, T. K. C. Hui, Y. Zhou, C. Li, D. Lei, K. H. Li, X. Wang, Q. Wang, L. Shao, Z. Chu, *Nat. Commun.* **2023**, *14*, 2507.

[14] a) R. Arppe, T. J. Sørensen, *Nat. Rev. Chem.* **2017**, *1*, 0031; b) P. Kustov, E. Petrova, M. Nazarov, A. Gilmullin, M. Sandomirskii, E. Ponkratova, V. Yaroshenko, E. Ageev, D. Zuev, *ACS Appl. Nano Mater.* **2022**, *5*, 10548; c) E. Ponkratova, E. Ageev, P. Trifonov, P. Kustov, M. Sandomirskii, M. Zhukov, A. Larin, I. Mukhin, T. Belmonte, A. Nominé, S. Bruyère, D. Zuev, *Adv. Funct. Mater.* **2022**, *32*, 2205859; d) J. H. Kim, S. Jeon, J. H. In, S. Nam, H. M. Jin, K. H. Han, G. G. Yang, H. J. Choi, K. M. Kim, J. Shin, S.-W. Son, S. J. Kwon, B. H. Kim, S. O. Kim, *Nat. Electron.* **2022**, *5*, 433.